Multiaxial deformation and strain-induced crystallization around a fatigue crack in natural rubber

Pierre Rublon, Bertrand Huneau, Erwan Verron, Nicolas Saintier, Stéphanie Beurrot, Adrien Leygue, Cristian Mocuta, Dominique Thiaudière, Daniel Berghezan

Multiaxial deformation and strain-induced crystallization around a fatigue crack in natural rubber

Pierre Rublon [a], Bertrand Huneau [a,*], Erwan Verron [a], Nicolas Saintier [b], Stéphanie Beurrot [a], Adrien Leygue [a], Cristian Mocuta [c], Dominique Thiaudière [c], Daniel Berghezan [d]

[a] *École Centrale de Nantes, Institut de Recherche en Génie Civil et Mécanique (GeM), UMR CNRS 6183, BP 92101, 44321 Nantes Cedex 3, France*
[b] *Arts et Métiers ParisTech, I2M-DuMAS, UMR CNRS 5295, Bordeaux, France*
[c] *Synchrotron Soleil, L'Orme des Merisiers, BP 48, 91192 Gif sur Yvette, France*
[d] *Michelin, Centre Technique de Ladoux, Clermont-Ferrand, France*

The study of fatigue crack propagation in elastomers is an essential prerequisite to improve the service life of tire products. Natural rubber is a key compound in tires, because of its unique mechanical properties and more particularly its remarkable resistance to fatigue crack growth as compared to synthetic rubbers. To explain this resistance, the literature often mentions the phenomenon of strain-induced crystallization which takes place at fatigue crack tips in natural rubber and then reinforces it. In the present study, an original experimental set-up that couples synchrotron radiation with a homemade mechanical fatigue machine is developed to investigate both strain-induced crystallization and deformation multiaxiality around fatigue cracks in natural rubber. During uninterrupted fatigue tests, recording of wide-angle X-ray diffraction patterns is performed in the crack tip region providing the two-dimensional spatial distribution of both crystallinity and principal strain directions. In particular, the influence of loading conditions on the size of the crystallized zone is investigated and related to fatigue crack growth rates. Finally, measurements of deformation multiaxiality, i.e. principal strain directions and change in thickness, obtained by this method are successfully compared with digital image correlation results.

Keywords:
Fatigue crack
Natural rubber
Strain-induced crystallization
Synchrotron radiation
Digital image correlation

1. Introduction

Because of its outstanding mechanical properties, particularly its fatigue resistance [1–3], Natural rubber (NR) is a key material in many industrial applications such as tires. In literature, its ability to crystallize under deformation (strain-induced crystallization, SIC [4]), in particular in the vicinity of crack tips where the material is largely strained [5–7], is classically invoked to explain longer service life and better fatigue crack growth resistance than synthetic elastomers. More precisely, authors argue that the crystallized rubber around the crack tip slows down crack growth [3]. However, the influence of this crystallized zone at crack tip on fatigue crack propagation remains still unproven.

In this context, the present paper aims to relate fatigue crack growth rates in NR samples with the characteristics of the crystallized zone around crack tip, and then to explain the macroscopic fatigue properties. In this way, three experimental methods are developed and their results are compared:

* Corresponding author. Tel.: +33 (0)2 40 37 68 82.
E-mail address: bertrand.huneau@ec-nantes.fr (B. Huneau).

Nomenclature

c	crack length
dc/dn	crack growth rate
h	thickness of the deformed PS sample
h_0	thickness of the undeformed PS sample
I_{200}	intensity of the X-rays diffracted by the (200) plane
$I_{amorphous}$	intensity of the X-rays diffracted by the amorphous part of the rubber
l	height of the deformed PS sample
l_0	height of the undeformed PS sample
n	number of cycles
T	tearing energy (or energy release rate)
w	strain energy
W_0	strain energy per unit undeformed volume
χ	index of crystallinity
Φ	angle of rotation of the principal strain direction
λ	stretch ratio in the tension direction for the PS sample
λ_3	stretch ratio in the out-of-plane direction (thickness) for the PS sample

Acronyms

CB	carbon black
DIC	digital image correlation
IR	isoprene rubber
IR50	isoprene rubber filled with 50 phr of carbon black
NR	natural rubber
NR50	natural rubber filled with 50 phr of carbon black
phr	parts per hundred of rubber
PS	pure shear
SIC	strain-induced crystallization
WAXD	wide-angle X-ray diffraction

- first, classical fatigue crack propagation tests are performed on different pre-cracked "pure shear" (PS) samples of NR filled with carbon black in order to evaluate crack growth rate;
- second, the strain field around the crack tip is evaluated by digital image correlation (DIC) measurements;
- third, in situ fatigue tests are conducted at the French national synchrotron facility SOLEIL in order to measure in real-time the crystallinity in the vicinity of the crack tip. The method consists in mapping the crack tip neighbourhood while recording wide-angle X-ray diffraction (WAXD) patterns; see [8] for details on its development. It permits the measurement of both SIC distribution and deformation state, i.e. principal strain directions and change in thickness, around the crack during uninterrupted fatigue tests.

2. Experimental method

2.1. Material and sample

The fatigue experiments are conducted with NR samples filled with 50 phr of N347 carbon black (CB). Vulcanization is carried out with 1.6 phr of sulphur together with CBS (N-Cyclohexyl-2-benzothiazole sulfonamide) that acts as an accelerator. Each blend also contains zinc oxide (ZnO) and stearic acid. 6PPD (N-(1,3-dimethylebutyl)-N′-phenyl-p-phenylenediamine) is used as an antioxydant. In addition, a synthetic isoprene rubber (IR) filled with 50 phr of CB N347 and with exactly the same amounts of additives than NR compound, is synthesized. As in this IR (89% of CIS configuration) SIC is considerably reduced compared to NR, the corresponding measurements are helpful to discuss SIC influence on fatigue crack growth properties. The formulation of NR and IR materials are given in Table 1. In the following, these two compounds will be denoted NR50 and IR50.

The geometry of the samples is a classical "pure shear" geometry (also known as planar tension samples), commonly employed for fatigue crack growth tests [9–11]. The dimensions are reported in Fig. 1.

2.2. Fatigue crack growth rate tests

Fatigue crack growth measurements are based on the energy balance approach of Rivlin and Thomas [12], who extended the concept of energy release rate of Griffith [13] to the case of non-linear hyperelastic materials. Considering thin planar

Table 1
Material formulation

Ingredients	Content (phr)	
NR	100	–
IR	–	100
Carbon black N347	50	50
Stearic acid	2	2
Zinc oxide	2.5	2.5
CBS accelerator	1.6	1.6
6PPD	1.9	1.9
Sulphur	1.6	1.6

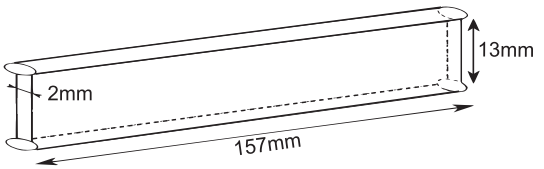

Fig. 1. Geometry and dimensions of "pure shear" samples.

samples of uniform undeformed thickness h_0, and denoting c the crack length, the "tearing energy" T, i.e. the denomination of energy release rate for rubber materials, is derived as

$$T = -\frac{1}{h_0}\frac{\partial w}{\partial c}\bigg|_l \tag{1}$$

where w is the strain energy and the suffix $\cdot_l$ denotes differentiation with constant displacement of the boundaries over which forces are applied. In the particular case of PS samples, they established the following relation between T, W_0 the strain energy density per unit undeformed volume, and l_0 the height of the undeformed sample

$$T = W_0 l_0 \tag{2}$$

Fatigue crack growth propagation experiments were performed at Michelin (Clermont-Ferrand, France) on a MTS servo-hydraulic fatigue machine at room temperature, in air and with a 2 Hz sinusoidal waveform. After clamping, the uncracked sample is first cycled during 300 cycles at a global stretch ratio $\lambda = l/l_0 = 1.92$, to suppress Mullins effect and lower the residual stretch mainly due to inherent viscous effects. Cyclic tests with uncracked samples are then conducted at different λ from 1.08 to 1.92; the strain energy density W_0 is then determined by integrating the area under the stress–strain curve.

After the creation of three pre-cracks (which entails four crack tips) in the sample at the edges (2 cm-long) and in the middle of the sample (3 cm-long), a short preliminary cyclic test is performed to blunt the crack tips and to transform cutter incisions into fatigue cracks. Afterwards, the procedure of fatigue crack growth experiments consists in cycling the cracked sample for different global stretch ratios (corresponding to different values of T). Cyclic tests are paused several times to measure the mean value of the crack extension dc of the four crack tips with a stereo microscope, from which we deduce the crack growth rate (dc/dn in nm per cycle). A conventional way to represent the results is a log–log dc/dn vs. T curve [2].

2.3. Digital image correlation (DIC)

The now well-established method of DIC leads to the measurement of the displacement field (and then the 2D strain field) in the vicinity of a fatigue crack tip in a stretched sample. Moreover, it also provides the principal strain directions. In the present study, the analysis of the displacement field near the crack tip is performed with the commercial DIC software Davis (edited by LaVision). The use of this method necessitates a good contrast on the surface of the sample; it is obtained by using a white talcum powder which provides a satisfactory distribution of gray levels. The acquisition of images is then performed by a Nikon D90 camera at different levels of extension and the pixel size on each photo is approximately 4 μm (see a typical example in Fig. 2).

2.4. In situ WAXD experiments

In situ WAXD measurements are conducted with a homemade fatigue machine using two electrical actuators which apply a cyclic sinusoidal extension to the rubber sample; this machine has been already used in a previous study [14]. It is fixed on a mobile diffractometer on the DiffAbs beamline at the French national synchrotron facility SOLEIL. The wavelength of the X-ray beam is 0.1305 nm and the beamsize is approximately 300 μm × 200 μm (full width at half maximum). The two-dimensional WAXD patterns are recorded by a MAR CCD X-ray detector (SX-165) with an exposure time of 1 s (see the typical pattern in Fig. 3). In the following, the equatorial direction is the direction that goes through the maximum of

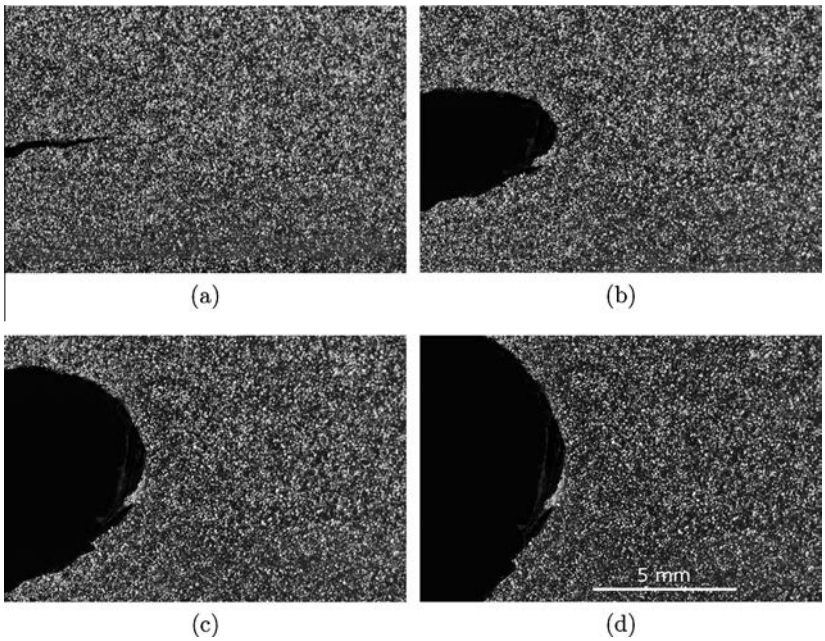

Fig. 2. Acquisition of images on a cracked sample of NR50 at different levels of extension for DIC analysis: (a) $\lambda = 1$, (b) $\lambda = 1.31$, (c) $\lambda = 1.67$, (d) $\lambda = 1.92$. See the common scale in the bottom right-hand corner.

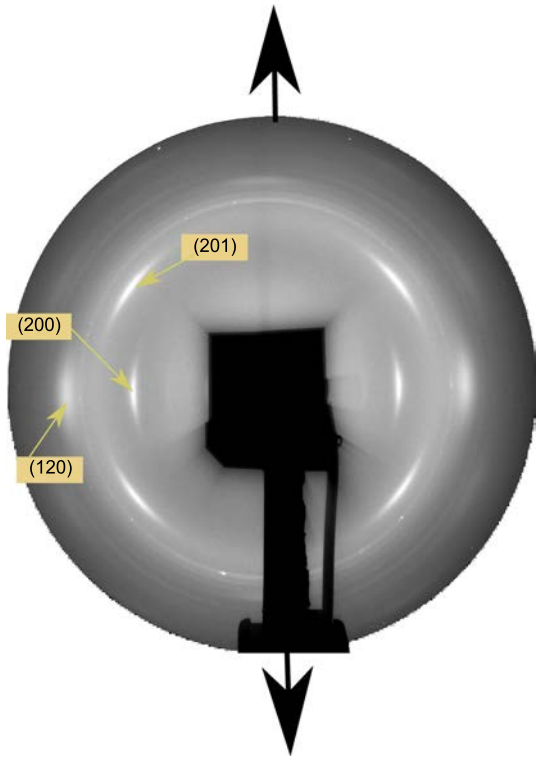

Fig. 3. Typical WAXD pattern. The black arrows indicate the tensile direction. The black shadow represents a direct beam blocker.

the two (200) reflections in azimuthal angle. The polar direction is simply defined as the perpendicular direction to the equatorial direction; it is parallel to the global stretching direction in Fig. 3 and more generally it corresponds to the maximum principal strain direction. The transmitted beam is blocked by a Pb beamstop on which a Si PIN photodiode is placed to measure the transmitted intensity through the rubber, and then retrieve the thickness of the sample. For in situ WAXD experiments, only one fatigue pre-crack is introduced in the sample. After the same accommodation procedure as the one performed for fatigue crack growth test, the WAXD acquisition starts. It consists in mapping the neighbourhood of the crack tip with WAXD measurement in 90 points (rectangular mapping of 9×10 points) without stopping the cyclic loading. Diffraction data are acquired at the top of each cycle (see Fig. 4) and the sample is moved with respect to the beam between two cycles in order to perform the next WAXD acquisition in the next point of the mapping. A minimum 1 s exposure time of the detector is needed to obtain satisfactory WAXD patterns with our experimental conditions. For this reason and in order to accurately displace the sample between two successive measurements, it is necessary to prescribe a low loading frequency, i.e. 0.1 Hz, during data acquisition. Each map contains 90 diffraction patterns; in fact, it is assumed that during those 90 cycles, the growth of the crack is negligible as compared to the mapping size in the fatigue crack propagation direction. This assumption has been verified *a posteriori* from the measurement of the crack length after each loading sequence; in any case the crack advance was smaller than 10% of the crystallized zone's length, in the crack propagation direction. Fig. 4 summarizes the procedure. For the sake of brevity, we do not present here the complete treatment of the data; interested reader can refer to [8] for details. However, it is to note that the calculation of the index of crystallinity has been improved compared with the procedure described in [8]. Indeed, in order to account for the oriented amorphous phase, the misorientation of crystallites (which leads to larger reflections) and the influence of carbon black fillers, we extract the total diffracted intensity (averaged over an azimuthal angle of 40°, whereas only 1° was considered in [8]), at azimuthal angles corresponding to the (200) and the (120) Bragg reflections. Then, we deconvolute the amorphous and crystallized peaks, and an additional peak due to the addition of CB with Pearson VII functions. The deconvolution of a typical pattern is shown in Fig. 5. Practically, an angle larger than 40° would have led to a longer and more difficult deconvolution due to the peaks corresponding to (201) reflections. Moreover the small peak besides the (120) peak was not considered in the deconvolution as it did not influence significantly the value of crystallinity. The index of crystallinity is then defined as

$$\chi = \frac{\int I_{200}}{\int I_{200} + \int I_{\text{amorphous}}} \tag{3}$$

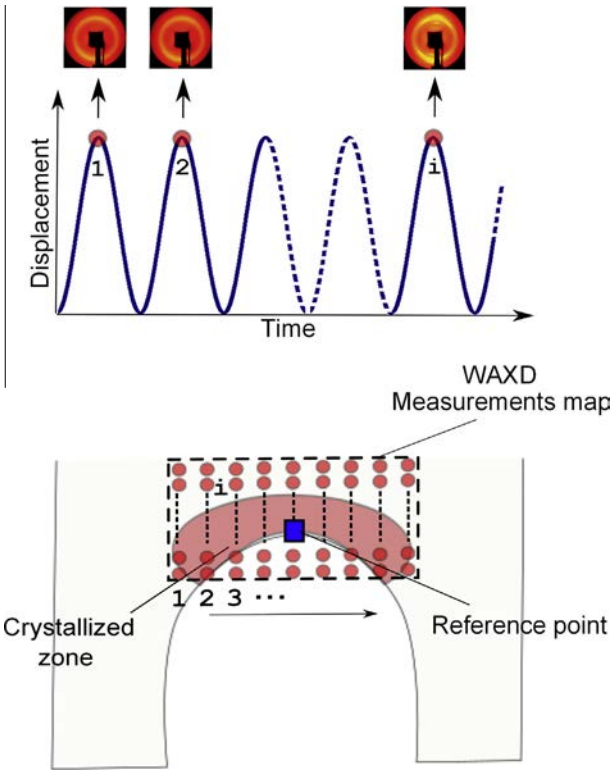

Fig. 4. WAXD measurements during fatigue tests. Top: each diffraction pattern is recorded at the maximum displacement of each cycle. Bottom: between two measurements, the sample moves with respect to the beam to reach the next point on the prescribed map. The arrow indicates the scan direction. The loading direction is horizontal.

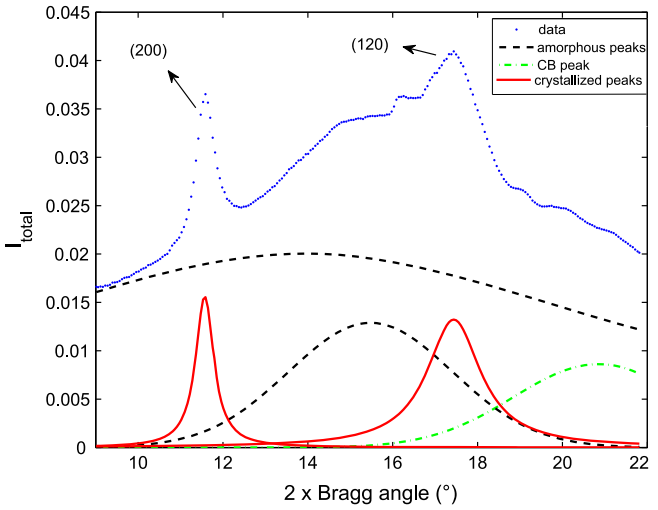

Fig. 5. Deconvolution and fitting of a pattern.

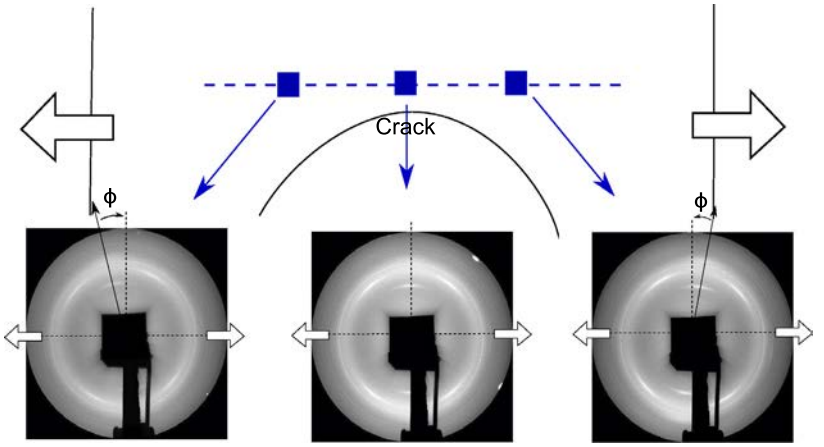

Fig. 6. Rotation of Bragg reflections nearby the crack tip in NR50 with $\lambda = 1.92$. It provides the mean orientation of crystallites and indirectly the rotation of principal strain directions.

where $\int I_{200}$ is the area under the (200) peak and $\int I_{\text{amorphous}}$ is the area under amorphous peaks. It is worth noting that the amorphous intensity is averaged in the polar and equatorial directions (for an azimuthal angle of 40° in each direction) which permits to take into account for the calculation of χ the orientation of the amorphous phase during sample stretching. However, this orientation has not been quantified here.

These measurements lead finally to the plot of iso-χ curves around the crack tip. Thus, it provides both size and shape of the crystallized zone. Moreover, considering the transmitted intensity as a measurement of the thickness, it is also possible to compute the volume of this crystallized zone around the crack tip. Finally, the rotation of principal directions near the crack tip is also measurable by considering the rotation of Bragg reflections of the different recorded WAXD patterns, as it was done by Pannier et al. [15]. Fig. 6 shows the rotation of the Bragg reflections in front of the crack tip. This rotation is quantified by the angle Φ.

3. Results and discussion

3.1. Fatigue crack growth rates

The fatigue crack growth properties of NR filled with 50 parts per hundred of rubber (phr) of CB is compared with the ones of IR filled with the same amount of carbon black. The crack growth rates are presented in Fig. 7. For a given tearing energy, the crack growth rate is lower for NR50 than for IR50; it is particularly noticeable for high values of tearing energy. This observation is confirmed by the slopes of the power law fits: 1.85 for NR50 and 2.73 for IR50. Nevertheless, crack growth

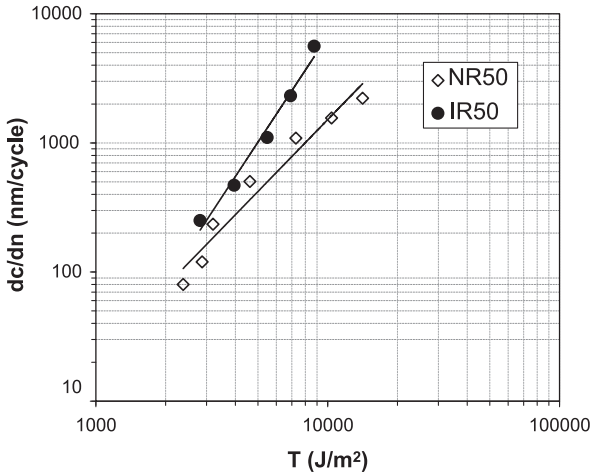

Fig. 7. Fatigue crack growth rates in NR50 (unfilled symbols) and IR50 (filled symbols).

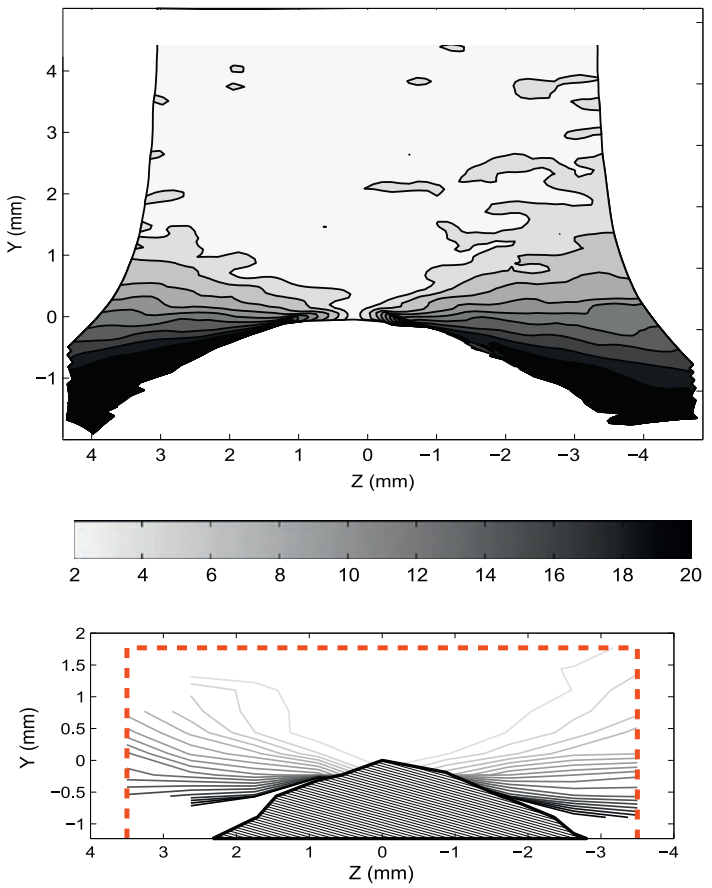

Fig. 8. Absolute value of the rotation angle Φ (in degrees) of the principal strain directions, corresponding to the maximum stretch ratio, with respect to the global stretching direction at crack tip measured by DIC (top) and WAXD (bottom) in NR50 with $\lambda = 1.92$ (deformed configuration). The grayscale applies to both plots.

rates for $T < 5000\,\mathrm{J/m^2}$ does not significantly differ. These results are in good agreement with previously published data: even if a comparison between highly different materials might be hazardous, we note that Lake [16] obtained similar results by comparing NR with SBR (styrene-butadiene rubber), a completely amorphous material.

3.2. Multiaxial deformation at crack tip

3.2.1. Principal strain directions

Fig. 8 shows the orientation of the principal strain directions measured by DIC and WAXD. This orientation corresponds to the angle Φ (see Fig. 6) which is the angle between the global stretching direction, and the direction of the maximum principal strain with respect to the undeformed configuration for each measurement point. Indeed, Φ represents the rotation of the principal strain directions induced by the crack tip because the normal-to-the-crack propagation direction is the principal strain direction that corresponds to the maximum stretch ratio in the uncracked sample.

To compare the two experimental techniques, Fig. 9 presents the distribution of Φ along the axis perpendicular to the crack direction at the crack tip (see axis Z in the figure). This figure emphasizes the very good agreement between the techniques; it also illustrates an original use of the WAXD results to investigate mechanical quantities at the local scale.

3.2.2. Change in thickness

A mapping of the change in thickness h/h_0 (which corresponds to the out-of-plane stretch ratio λ_3), with h the deformed thickness at a given point, is proposed in Fig. 10; this result is obtained by the transmitted X-ray beam for a NR50 sample with a global stretch ratio $\lambda = 1.92$. As expected, it highlights the substantial change in thickness in the vicinity of the crack tip, as compared to the global change in thickness far from it. To quantify this difference, Fig. 11 presents the change in thickness along two axes which cross at crack tip. The data obtained by transmitted X-ray beam are compared with those obtained by DIC. More precisely, for the latter method the change in thickness is calculated from the in-plane strain measures and considering the incompressibility assumption for the material. The very good agreement of the measurements permits first to conclude on the relevance of the transmitted X-ray beam method to evaluate the out-of-plane strain but also to validate the in-plane strain measured from DIC, even near the crack tip. Second, the comparison of the results from the two methods validate the incompressibility assumption classically adopted for rubber-like materials [17–19] even in the near crack tip region. Nevertheless, it is thought by the authors that, if the material is not perfectly incompressible, the deviation from incompressibility would be small especially if one considers that the effect of SIC would counterbalance the effect of cavitation. This point was investigated by Chenal et al. [20]. According to this author, the volume variation is less than 2.5% in a filled NR after a few cycles (i.e. after Mullins effect). Consequently, it would not have a significant influence on the curves given in Fig. 11.

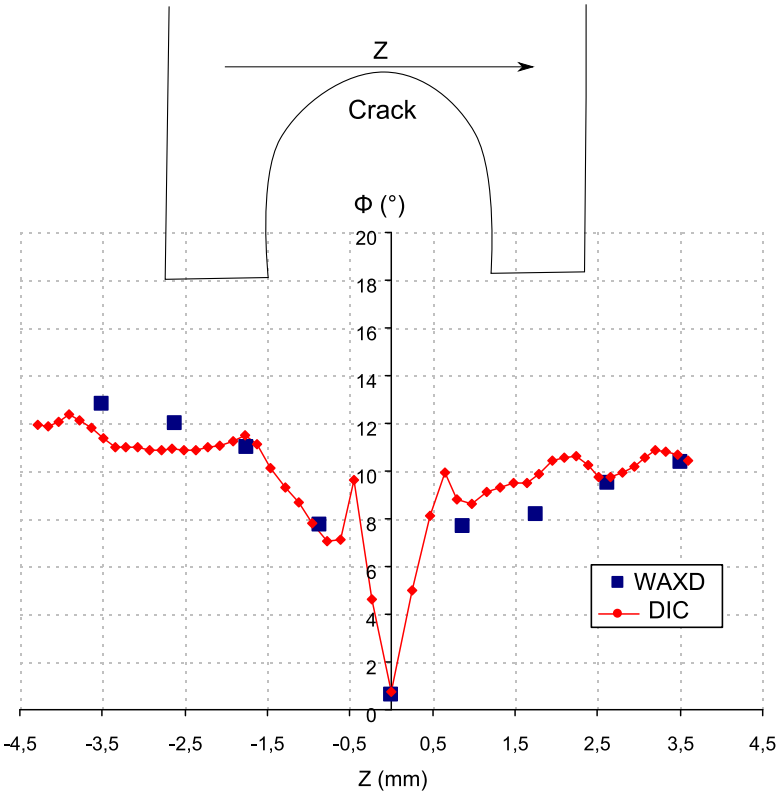

Fig. 9. Distribution of Φ measured by DIC and WAXD in front of the crack tip along an axis perpendicular to the crack propagation in NR50 with $\lambda = 1.92$ (deformed configuration).

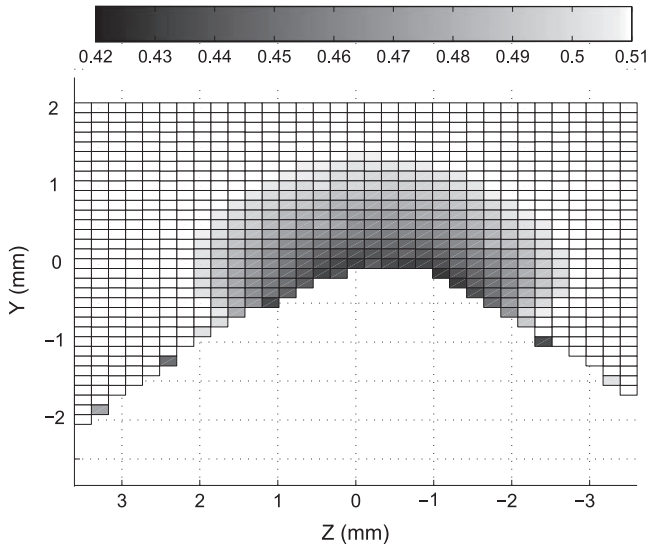

Fig. 10. Change in thickness h/h_0 in the vicinity of the crack tip, as deduced from measuring the transmitted X-ray beam in NR50 with $\lambda = 1.92$ (deformed configuration).

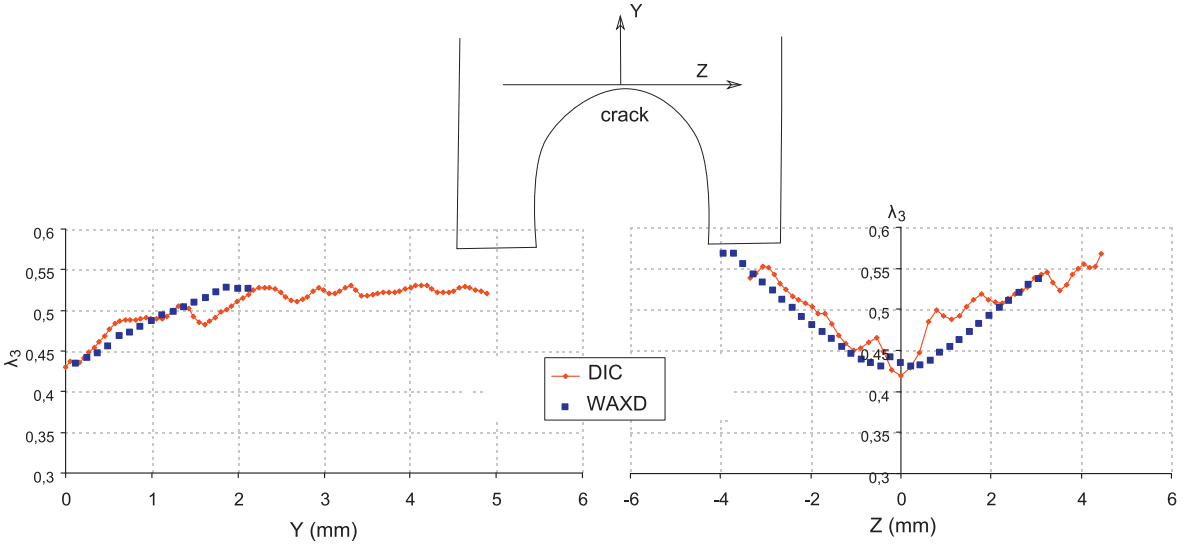

Fig. 11. Change in thickness $\lambda_3 = h/h_0$ in the vicinity of the crack tip: in the crack direction (Y) and in the direction normal to the crack (Z) in NR50 with $\lambda = 1.92$ (deformed configuration). We recall that λ_3 corresponds to the out-of-plane stretch ratio.

3.3. Crystallized zone at crack tip

3.3.1. Size of the crystallized zone

Fig. 12 presents the iso-crystallinity plots obtained after the WAXD measurements around the fatigue crack tip of NR50 samples for four different values of T. It logically emphasizes the influence of this parameter on the size of the crystallized zone: as the global stretch ratio increases, the local strain levels increase in the vicinity of the crack and then more matter crystallizes. These results corroborate the ones of Lee and Donovan [5], Trabelsi et al. [6]; and also Brüning et al. [7], whose measurements of SIC where performed in dynamic conditions. All those studies report an enlargement of the crystallized zone for a carbon black filled NR [5,7] and an unfilled NR [6], respectively. Nevertheless, quantitative comparisons with these results are not possible, because experimental conditions, i.e. materials, samples geometry and loading conditions, noticeably differ.

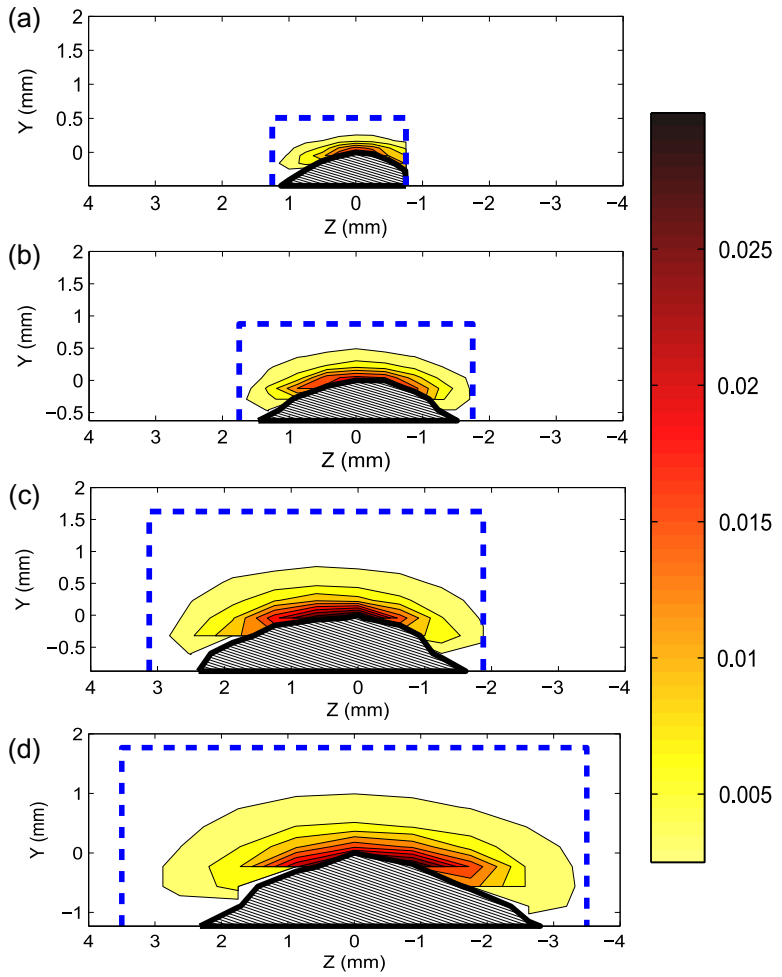

Fig. 12. Distribution of the index of crystallinity around a fatigue crack tip in NR50 for four different values of tearing energy (deformed configuration): (a) $T = 4620\,\mathrm{J/m^2}$, (b) $T = 7290\,\mathrm{J/m^2}$, (c) $T = 10,390\,\mathrm{J/m^2}$, (d) $T = 14140\,\mathrm{J/m^2}$. The lowest value of the index is 0.0025; it corresponds to the threshold of detection.

Furthermore, it is to note that the frequency decrease (from 2 to 0.1 Hz) applied to perform the acquisition and the mapping might have a slight effect on the observed results. Recent studies dealing with the kinetics of SIC [21–23] have highlighted that the crystallization characteristic time in NR is short, around 20 ms according to Candau et al. [21], which is much smaller than the duration of a half fatigue cycle at 2 Hz (250 ms). It means that SIC still exists at 2 Hz especially when the distance to the crack tip is reduced because the stretch ratios are very high. However, according to Candau et al. [21] this characteristic time can rise to 200 ms when the stretch ratio is close to the onset of crystallization, which means that the crystallized zone is smaller in real fatigue conditions (2 Hz) compared with the one measured at 0.1 Hz.

3.3.2. Relationship between T and crystallinity

In order to propose a preliminary result on the influence of SIC on fatigue crack growth, one can compare the crack growth and the quantity of matter that is crystallized. In this way, the volume of matter that contains crystals around the crack tip is computed by multiplying the surface of the crystallized zone by the deformed thickness measured by the transmitted intensity measurement presented above. Fig. 13 presents the evolution of this quantity with respect to the tearing energy.

In order to comment this figure, we recall the results of Fig. 7 which compares the crack growth rate of NR and IR. It is to note that IR does almost not crystallize when stretched, thus it is not plotted in Fig. 13. On the one hand, the resistance to fatigue crack growth in NR is greater than the one in IR, and it is all the more true for high values of T. On the other hand, the volume of the crystallized zone at crack tip in NR increases with T. It tends to prove that SIC slows down crack growth. To sum up: the higher the tearing energy, the larger the crystallized zone at crack tip and the lower the crack growth rate in NR as compared to IR.

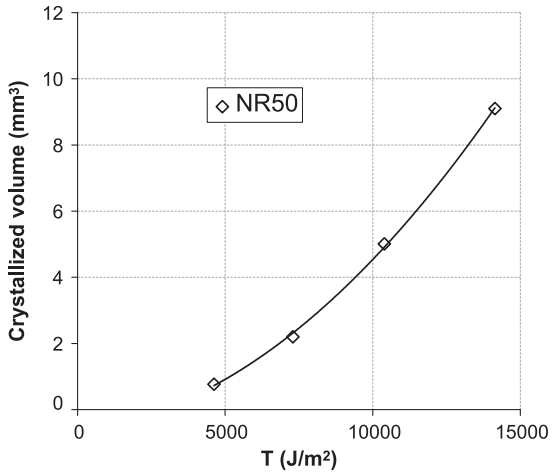

Fig. 13. Volume of the crystallized zone around crack tip as a function of tearing energy for NR50. The line represents a fitted power law.

4. Conclusion

In this paper, the multiaxiality of strain and the strain-induced crystallization in the vicinity of a fatigue crack tip have been investigated thanks to both the DIC technique and an original experimental set-up, which consists in the association of a homemade fatigue machine with synchrotron WAXD. The discussion of these experimental results with respect to fatigue crack growth rates permits to emphasize the influence of crystallinity on crack growth in filled elastomers, and leads to an explanation of the remarkable resistance to fatigue crack growth of natural rubber.

As a conclusion, the contributions of this work are twofold. First, from a methodological point of view, the interest of using WAXD technique to measure crystallinity, principal strain directions and out-of-plane strain has been demonstrated. We can also argue that our WAXD study validates both in-plane DIC measurements and incompressibility assumption. Second, as a preliminary result, we have established a simple relationship between the tearing energy and the crystallized volume in the vicinity of the crack tip. This first quantitative result paves the way for further investigation on strain-crystallizing elastomers in fatigue: comparison of materials, influence of carbon black reinforcement and effect of complex loading conditions.

References

[1] Cadwell SM, Merril RA, Sloman CM, Yost FL. Dynamic fatigue life of rubber. Rubber Chem Technol 1940;13:304–15.
[2] Lake G. Fatigue and fracture of elastomers. Rubber Chem Technol 1995;68:435–60.
[3] Mars WV, Fatemi A. Factors that affect the fatigue life of rubber: a literature survey. Rubber Chem Technol 2004;77:391–412.
[4] Huneau B. Strain-induced crystallization of natural rubber: a review of X-ray diffraction investigations. Rubber Chem Technol 2011;84:425–52.
[5] Lee DJ, Donovan JA. Microstructural changes in the crack tip region of carbon-black-filled natural rubber. Rubber Chem Technol 1987;60:910–23.
[6] Trabelsi S, Albouy P-A, Rault J. Stress-induced crystallization around a crack tip in natural rubber. Macromolecules 2002;35:10054–61.
[7] Brüning K, Schneider K, Roth SV, Heinrich G. Strain-induced crystallization around a crack tip in natural rubber under dynamic load. Polymer 2013;54:6200–5.
[8] Rublon P, Huneau B, Saintier N, Beurrot S, Leygue A, Verron E, et al. In situ synchrotron wide-angle X-ray diffraction investigation of fatigue cracks in natural rubber. J Synchrotron Radiat 2013;20:105–9.
[9] Young DG. Dynamic property and fatigue crack propagation research on tire sidewall and model compounds. Rubber Chem Technol 1985;58:785–805.
[10] Papadopoulos IC, Thomas AG, Busfield JJC. Rate transitions in the fatigue crack growth of elastomers. J Appl Polym Sci 2008;109:1900–10.
[11] Andreini G, Straffi P, Cotugno S, Gallone G, Polacco G. Crack growth behavior of styrene-butadiene rubber, natural rubber, and polybutadiene rubber compounds: comparison of pure-shear versus strip tensile test. Rubber Chem Technol 2013;86:132–45.
[12] Rivlin RS, Thomas AG. Rupture of rubber. J Polym Sci 1953;10:291–318.
[13] Griffith A. The phenomena of rupture and flow in solids. Philos Trans Roy Soc Lond A 1921;221:163–98.
[14] Beurrot-Borgarino S, Huneau B, Verron E, Rublon P. Strain-induced crystallization of carbon black-filled natural rubber during fatigue measured by in situ synchrotron X-ray diffraction. Int J Fatigue 2013;47:1–7.
[15] Pannier Y, Proudhon H, Mocuta C, Thiaudière D, Cantournet S. In situ multi-axial loading frame to probe elastomers using X-ray scattering. J Synchrotron Radiat 2011;18:907–11.
[16] Lake GJ. Mechanical fatigue of rubber. Rubber Chem Technol 1972;45:309–28.
[17] Treloar LRG. The physics of rubber elasticity. Oxford: Oxford University Press; 1975.
[18] Ogden RW. Non-linear elastic deformations. Chichester: Ellis Horwood; 1984.
[19] Holzapfel GA. Nonlinear solid mechanics. A continuum approach for engineering. Chichester: J Wiley and Sons; 2000.
[20] Chenal JM, Gauthier C, Chazeau L, Guy L, Bomal Y. Parameters governing strain induced crystallization in filled natural rubber. Polymer 2007;48:6893–901.
[21] Candau N, Chazeau L, Chenal JM, Gauthier C, Ferreira J, Munch E, et al. Characteristic time of strain induced crystallization of crosslinked natural rubber. Polymer 2012;53:2540–3.
[22] Albouy PA, Guillier G, Petermann D, Vieyres A, Sanseau O, Sotta P. A stroboscopic X-ray apparatus for the study of the kinetics of strain-induced crystallization in natural rubber. Polymer 2012;53:3313–24.
[23] Brüning K, Schneider K, Roth SV, Heinrich G. Kinetics of strain-induced crystallization in natural rubber studied by WAXD: dynamic and impact tensile experiments. Macromolecules 2012;45:7914–9.